ARTICLES
PUBLISHED ONLINE: 17 MARCH 2013 | DOI: 10.1038/NNANO.2013.26
nature nanotechnology

Large tunable image-charge effects in single-molecule junctions

Mickael L. Perrin[1], Christopher J. O. Verzijl[1], Christian A. Martin[1], Ahson J. Shaikh[2], Rienk Eelkema[2], Jan H. van Esch[2], Jan M. van Ruitenbeek[3], Joseph M. Thijssen[1], Herre S. J. van der Zant[1]* and Diana Dulić[1]

Metal/organic interfaces critically determine the characteristics of molecular electronic devices, because they influence the arrangement of the orbital levels that participate in charge transport. Studies on self-assembled monolayers show molecule-dependent energy-level shifts as well as transport-gap renormalization, two effects that suggest that electric-field polarization in the metal substrate induced by the formation of image charges plays a key role in the alignment of the molecular energy levels with respect to the metal's Fermi energy. Here, we provide direct experimental evidence for an electrode-induced gap renormalization in single-molecule junctions. We study charge transport through single porphyrin-type molecules using electrically gateable break junctions. In this set-up, the position of the occupied and unoccupied molecular energy levels can be followed *in situ* under simultaneous mechanical control. When increasing the electrode separation by just a few ångströms, we observe a substantial increase in the transport gap and level shifts as high as several hundreds of meV. Analysis of this large and tunable gap renormalization based on atomic charges obtained from density functional theory confirms and clarifies the dominant role of image-charge effects in single-molecule junctions.

In self-assembled monolayers, the influence of the molecule/metal interface on the alignment of the molecular orbital level with respect to the Fermi energy of the substrate has been extensively studied with ultraviolet and X-ray photo-emission spectroscopy[1–4], Kelvin probe measurements[5,6], and scanning tunnelling microscopy[7]. Such measurements have indicated the formation of an interfacial dipole that is associated with substantial workfunction shifts[1–5,7], which affect all molecular orbitals in a similar way. Several mechanisms have been identified that could cause this interfacial dipole. In physisorbed systems, the compression of the tail of the electron density outside the metal (the 'pillow' or 'push-back' effect) plays an important role; whereas for chemisorbed systems, charge transfer also causes a surface dipole near the metal/molecule interface[1,3,8,9]. Additionally, straining the molecular junction may shift the orbital levels[10]. Upon stretching or compression of the molecular junction, the shifts of the occupied and unoccupied levels were found to be nearly uniform for the frontier orbitals[11]. Finally, the interaction of the (almost) neutral molecule with its own image-charge distribution at zero bias may also lead to a uniform level shift. This effect is present in both physisorbed and chemisorbed systems.

In contrast to the previously mentioned effects, ultraviolet photo-emission spectroscopy experiments probing the ionization and electron addition energies for decreasing layer thicknesses[12] have shown that the occupied levels move up and the unoccupied ones down in energy; this is called 'gap renormalization'. Transport gap renormalization has also been observed in single-molecule devices[13,14] and is commonly explained by the formation of image charges in the metal following the addition or removal of electrons from the molecule[15–17]. This effect occurs repeatedly when a current is passing through the molecule and is particularly apparent in molecules that are weakly coupled to the electrodes.

When varying the electrode separation, the molecular orbital levels are therefore subject to a uniform shift, combined with gap renormalization. Hence, distinguishing the dominant trend in single-molecule junctions requires the combination of an adjustable electrode separation with an electrostatic gate. Although mechanical control over molecular conductance has been reported in a number of studies[7,10,18–23], in only very few reports has it been combined with an electrostatic gate[18,19]. In particular, there is a lack of systematic studies based on explicit monitoring of the dependence of occupied and unoccupied orbital levels on molecule–electrode distance.

Current–voltage characteristics

We have investigated the influence of the metal electrodes on the energy levels in single-molecule junctions using two- and three-terminal mechanically controllable break junctions (MCBJs) in vacuum at 6 K. This architecture (shown in Fig. 1b) allows the distance between the electrodes to be tuned with picometre precision by bending the flexible substrate supporting partially suspended electrodes[24–30]. In three-terminal MCBJ devices an additional gate electrode allows electrostatic tuning of the energy levels of the molecular junction[19]. In this study, we used thiolated porphyrins, because they offer great architectural flexibility and rich optical properties. The thiol-terminated zinc-porphyrin molecules [Zn(5,15-di(p-thiolphenyl)-10,20-di(p-tolyl)porphyrin)] (Fig. 1a), abbreviated ZnTPPdT, were dissolved in dichloromethane (0.1 mM) and deposited on the unbroken electrodes using self-assembly from solution. The electrodes were then broken in vacuum at room temperature, and cooled. Current/voltage I–V characteristics were then recorded as a function of electrode spacing. All measurements were performed at 6 K. Details concerning these 'systematic I–V series' and other experimental procedures (synthesis of the molecules, measurement set-up and so on) are provided in Supplementary Sections SI–SVI.

[1]Kavli Institute of Nanoscience, Delft University of Technology, Lorentzweg 1, 2628 CJ Delft, The Netherlands, [2]Department of Chemical Engineering, Delft University of Technology, Julianalaan 136, 2628 BL Delft, The Netherlands, [3]Kamerlingh Onnes Laboratory, Leiden University, Niels Bohrweg 2, 2333 CA Leiden, The Netherlands. *e-mail: H.S.J.vanderZant@tudelft.nl

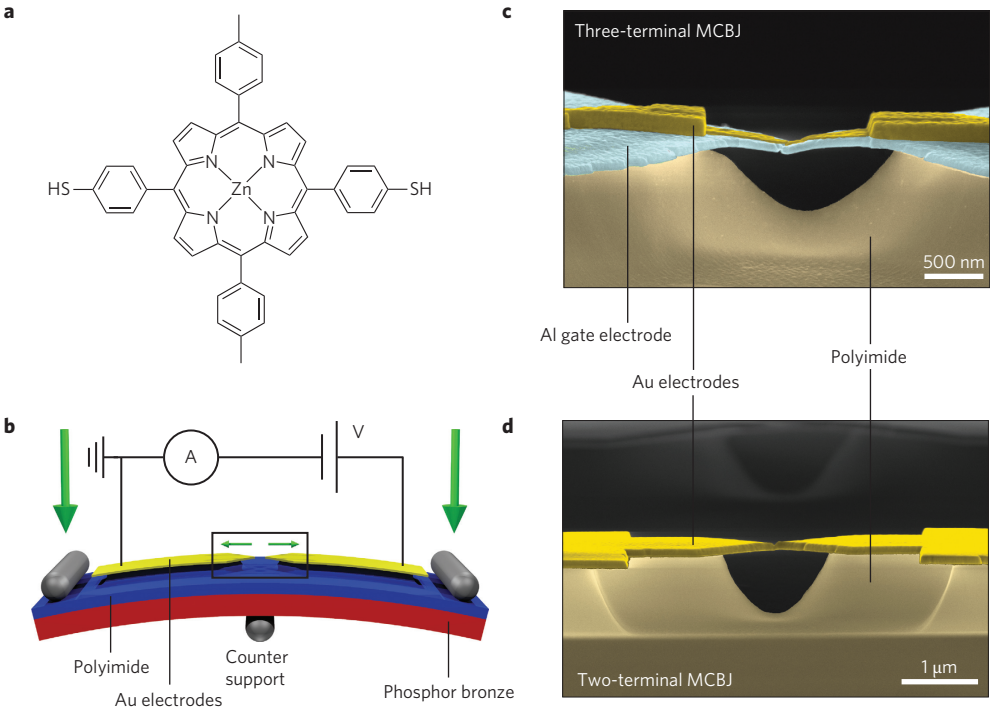

Figure 1 | Illustration of the experiments. a, Structural formula of ZnTPPdT. **b**, Layout of the MCBJ set-up. **c**, False colour scanning electron microscope (SEM) image of a three-terminal MCBJ device. The gate is made of aluminium and covered with a plasma-enhanced native aluminium oxide layer. The gold electrodes are deposited on top of the gate dielectric. **d**, False colour SEM image of a two-terminal MCBJ.

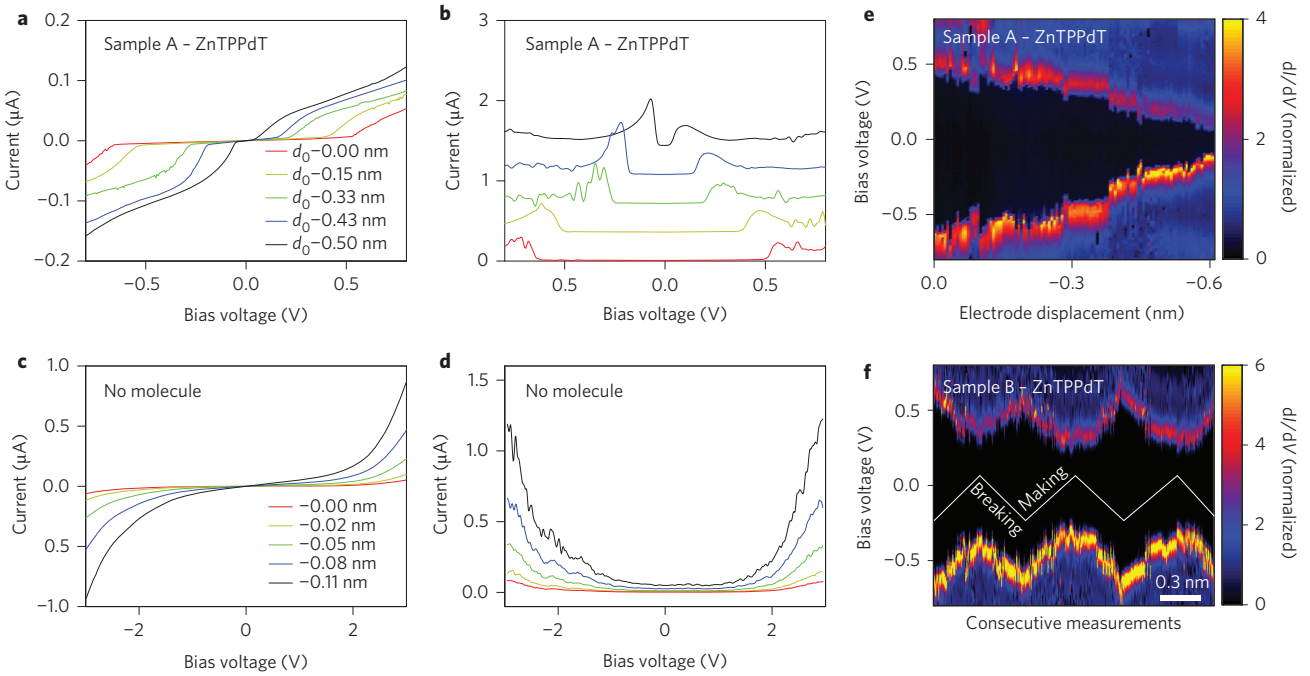

Figure 2 | Mechanical gating of charge transport in ZnTPPdT junctions. a,**b**, Current–voltage characteristics (**a**) and differential conductance (**b**) for MCBJ devices that have been exposed to a solution of ZnTPPdT. The estimated electrode displacement is relative to d_0, the initial electrode separation. **c**,**d**, The same quantities are plotted for junctions exposed to the pure solvent. **e**,**f**, Two-dimensional visualization of dI/dV for ZnTPPdT as a function of bias voltage and electrode displacement while fusing sample A (**e**) and for three making/breaking cycles of a different device (sample B) (**f**). A clear dependence of the Coulomb gap on electrode spacing is apparent. The differential conductance has been normalized.

Figure 2a presents typical I–V characteristics of a two-terminal MCBJ (sample A) that has been exposed to a solution of ZnTPPdT. We start monitoring the junction breaking or fusing process at electrode separation d_0. All characteristics show very low current around zero bias, indicating that transport occurs in the weak-coupling (Coulomb-blockade) regime. Steps at higher bias mark the transition to sequential tunnelling transport[31]. In the differential conductance dI/dV, these steps are visible as peaks (Fig. 2b). The peak location identifies the position of the molecular orbital level with respect to the Fermi energy of the electrodes. From here on we will refer to these peaks as

resonances. Figure 2a,b shows that, with decreasing inter-electrode distance, the spacing between the resonances is strongly reduced.

We have studied eight different junctions, and all displayed similar mechanically tunable resonances in dI/dV. Devices exposed to pure solvent, in contrast, showed featureless characteristics, typical of vacuum tunnelling through a single barrier (Fig. 2c,d). As the inter-electrode distance is reduced, the maximum current in these clean junctions increases smoothly as a result of the decreasing tunnelling barrier width.

To visualize the systematic evolution of the resonance position for hundreds of dI/dV curves we plotted a two-dimensional map of consecutive I–V measurements (Fig. 2e). In this plot, the gradual shift of the resonances becomes even more apparent. Owing to the stability of the electrodes and the fine control over their spacing[32,33], the energy levels can be shifted over several hundreds of meV by purely mechanical means.

In the following, we will refer to these shifts as 'mechanical gating' and quantify them in terms of an efficiency factor, 'mechanical gate coupling'. The mechanical gate coupling is expressed in units of V nm^{-1} and defined as the ratio between the shift of each resonance and the electrode displacement required to achieve this shift. From Fig. 2e, for example, we find a mechanical gate coupling of ~1 V nm^{-1}, with a slight asymmetry for positive and negative bias that may be caused by differences in capacitive coupling to the two electrodes. The reverse process (opening the junction) leads to a widening of the Coulomb gap, as illustrated in Fig. 2f, where several consecutive opening and closing cycles are shown for a different sample. This figure clearly shows that the resonances shift consistently and with similar magnitudes, demonstrating the robustness of the effect and the stability of the set-up.

While recording systematic I–V series, we occasionally observed a very weak dependence of the resonance positions on electrode separation. Conversely, we occasionally observed mechanical gate couplings as large as 1.5 V nm^{-1} (see Supplementary Section SVII for the statistics of the mechanical gate couplings). This is probably due to a rearrangement of the molecule inside the junction[32,34]. Alongside gradual changes in the position of the resonances, the plots in Fig. 2e,f display sudden irreversible jumps in the dI/dV data. These differences and variations could be caused by atomic-scale changes in the geometry of the molecular junction. Evidence of similar rearrangements has also been obtained during room-temperature conductance measurements on porphyrin molecules[34]. Throughout all the samples, however, the trends remain the same: reducing the electrode distance brings the resonances closer together, whereas increasing the distance moves them further apart.

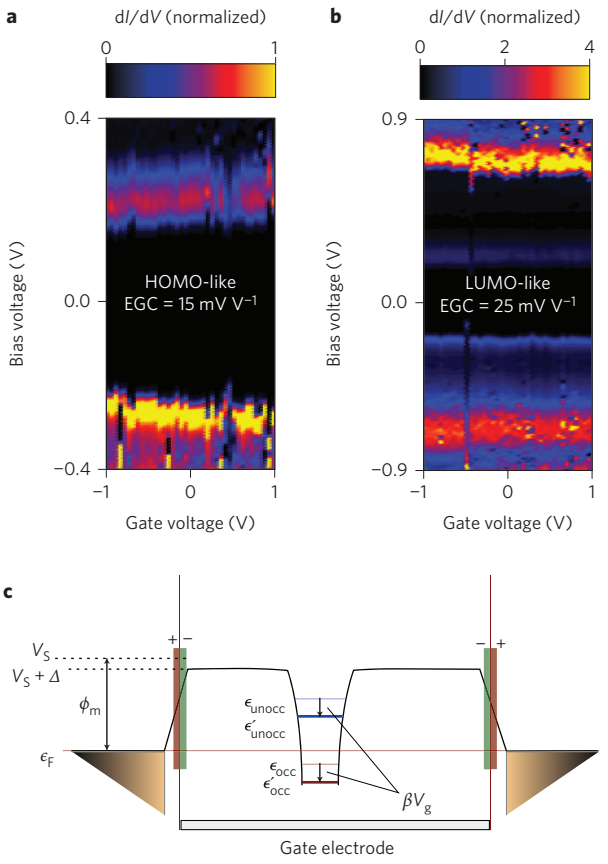

Figure 3 | Level shifts by electrostatic gating. a,**b**, Gate diagrams recorded on sample C for different junction configurations and during different breaking events. Colour-coded dI/dV plotted versus gate and bias voltage. The dependence of the resonance shift on gate voltage allows us to attribute resonances in **a** to an occupied level (HOMO-like, located at ~0.3 eV for zero gate voltage) and those in **b** to an unoccupied level (LUMO-like, located at ~0.75 eV for zero gate voltage). The corresponding electrostatic gate coupling value (EGC) is given in the figure. **c**, Effect of a rigid shift of the levels under electrostatic gating by a potential V_g applied to a gate electrode below the junction for an occupied and unoccupied level. Here, β is the electrostatic gate coupling, ϕ_m the metal workfunction, Δ is the shift of the potential V_S outside the surface due to the presence of the molecule, and ϵ_F is the Fermi energy of the metal. ϵ_{occ}, ϵ_{unocc} and ϵ'_{occ}, ϵ'_{unocc} are the occupied and unoccupied levels for $V_g = 0$ and $V_g \neq 0$, respectively.

Gate diagrams

To obtain additional information about the origin of the shifts of the molecular orbital levels involved in charge transport, we used electrically gated mechanical break junctions[19]. The electrostatic gate in these devices controls the potential on the molecule and lowers/raises all molecular orbital levels for positive/negative gate voltage[31], as shown in Fig. 3c. Keeping the electrode spacing fixed, we measured the current as a function of both the bias and gate voltage, and plotted dI/dV as a two-dimensional map. In this Article we will refer to such a plot as a 'gate diagram'.

In such a gate diagram the resonances associated with an occupied level move away from the Fermi level with increasing gate voltage. An unoccupied level, on the other hand, moves closer to the Fermi level and thus displays the opposite trend. This allows us to identify the resonance in Fig. 3a as the highest occupied molecular orbital (HOMO), whereas Fig. 3b shows an unoccupied level (this is not the lowest unoccupied molecular orbital (LUMO) of the gas phase molecule, as explained below). The HOMO level position depends on the gate voltage with an electrostatic gate coupling of ~15 mV V^{-1}; for the unoccupied level, we find an electrostatic gate coupling of ~25 mV V^{-1}. Figure 4a–b shows the mechanical gate plots recorded immediately after the measurements shown in Fig. 3a and b, respectively. Both the occupied and unoccupied levels move away from the Fermi level as we increase the distance between the electrodes (mechanical gate coupling is 0.40 V nm^{-1} for the occupied and 0.18 V nm^{-1} for the unoccupied level). This implies a widening of the gap and indicates that the mechanism behind the shifts cannot be a rigid change in the workfunction only, but must also include transport gap renormalization. It is the combination of electrostatic and mechanical gating that leads us to this conclusion, and in the following we will demonstrate, using density functional theory (DFT)-based calculations, that this gap renormalization is caused by the formation of image charges upon charge addition to/removal from the molecule.

Density functional theory calculations

We now turn to the theoretical analysis of the experimentally observed phenomena. Using a quantum chemistry approach[35] we studied the electronic structure of the molecules in the gas phase and sandwiched between gold atoms in the junctions, as well as

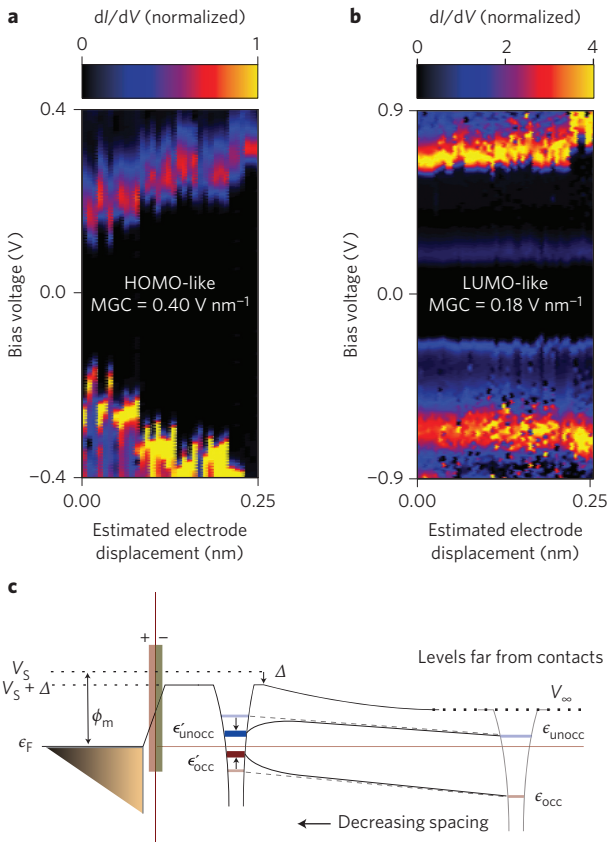

Figure 4 | Level shifts by mechanical gating. a,**b**, Systematic *I*–*V* series for sample C, recorded immediately after Fig. 3a and b, respectively. HOMO-like (located at ~0.3 eV for zero displacement), **a**) and LUMO-like (located at ~0.75 eV for zero displacement, **b**) levels both move away from the Fermi energy with increasing electrode spacing. The corresponding mechanical gate coupling value (MGC) is displayed. **c**, Shift of occupied and unoccupied molecular orbital levels with distance to the metal. The effects contained in Δ shift all levels in the same direction, while image-charge effects are responsible for occupied and unoccupied levels moving closer to the Fermi energy of the metal (gap renormalization). ϕ_m represents the metal workfunction, Δ the interfacial dipole, V_∞ the potential at infinity, V_S the potential at the surface and ϵ_F the Fermi energy. ϵ_{occ}, ϵ_{unocc} and ϵ'_{occ}, ϵ'_{unocc} are now the occupied and unoccupied levels of the molecule in the gas phase and at the interface, respectively.

their transport properties (for details see Supplementary Sections SIX and SX). In agreement with the literature, our calculations predict a chemisorbed system[36–38] with ZnTPPdT acting as acceptor, and the hollow site as the most stable configuration. Figure 5 shows the computed zero-bias transmission of the single-molecule junction using the non-equilibrium Green's function (NEGF) formalism. We find that the low-bias transport is dominated by the HOMO and HOMO-2 states of the molecule coupled to gold atoms (illustrated in Fig. 5a), which are visible as peaks in the transmission near the Fermi level.

We also observe that the resonances that correspond to the gas-phase LUMO and LUMO + 1 levels are located far above the Fermi level of the leads (although the precise location of these resonances cannot be predicted accurately with DFT). Being more strongly localized at the centre of the molecule than the better-hybridizing HOMO-like orbitals, both unoccupied levels are expected to have poor conductance properties and, as a consequence, are characterized by very narrow peaks in the calculations. A few additional peaks occur slightly above the Fermi energy, and inspection of these states reveals that they have no direct gas-phase counterpart. They are new states, which essentially consist of those parts of the gas-phase HOMO and LUMO that are located on the arms of the molecule and stabilized by the presence of the interface. Application of a positive gate voltage forces an extra electron into the molecule, and calculations indeed show that the charge is added to these levels, rather than to a LUMO state.

As discussed above, there is a correction Δ to the background potential that represents a workfunction shift, as illustrated in Fig. 4c. This shift is usually treated empirically, and on gold surfaces is typically negative. Experiments have reported shifts in the range −0.5 to −1 eV for H_2TPP and ZnTPP films[1,8], without the presence of the thiols in ZnTPPdT. In principle, this correction is distance-dependent and leads to a uniform shift in the occupied and unoccupied levels. This is in contrast with the experimentally observed gap renormalization, indicating that, although this effect may, to some extent, be present, it is not the dominant mechanism responsible for the large level shifts.

Image-charge effects, including their contribution to gap renormalization, can, in principle, be assessed by performing GW calculations[16,39,40], which allow for the determination of the ionization potentials and electron addition energies. However, such calculations are not feasible for the large molecules of this study. Instead, we calculate image-charge effects using classical electrostatics based on the atomic charges on the molecule obtained from DFT. In the region where the transport is blocked (corresponding to zero bias and gate) the molecule is approximately, but not exactly, neutral. We call this the 'reference state'. The combination of the negatively charged thiols and the positive core of the molecule in the reference state can lead to a contribution of the image charges effect to the uniform shift. This contribution either moves the levels up or down, depending on the exact charge distribution in the junction. To include gap renormalization, one also has to consider the different charged states of the molecule. To access the different charge states in the junction, we added or removed one electron from the molecule by applying a local gate field, in the spirit of a Δ–SCF method (for details see Supplementary Section SXI and ref. 41). The image-charge effect corrections are calculated for the different charge states by summing the electrostatic interactions of the atomic charges between two parallel plates with all image charges. The position of the image plane is taken to be 1.0 ± 0.25 Å outside the metal surface, as is usual in the literature[42–44]. For comparison with experiment, the distance between the electrodes has been varied.

The calculated shifts, illustrated in Fig. 5c, predict an image-charge contribution to the mechanical gate coupling in the range 1.1–2.8 V nm^{-1} for an occupied level and 0.4–2.1 V nm^{-1} for an unoccupied level, depending on electrode separation. The different molecular orbital levels (Fig. 5a) thus experience different image-charge effects, as observed in the experiments, although the calculated mechanical gate couplings are larger than the experimental ones. This can be due to the sharp contacts in the MCBJ experiment, which imply a smaller image-charge effect than the large parallel-plate contacts used in the calculation. We modelled the reduction of the image-charge effect with finite contacts, finding it to be a factor of ~1.5–2 (for details see Supplementary Section SXII), bringing the calculations into better agreement with the experimental shifts. To investigate the sensitivity to the orientation of ZnTPPdT in the junction, we also rotated the molecule in the calculations and found that the shifts remain essentially the same for angles within 45°.

To assess the contribution to the molecular orbital level shifts originating from structural deformation of the molecule, we performed DFT calculations for increasing gold–gold distance while letting the molecule relax between the contacts (for details see Supplementary Section SXIII). We found that the energy shifts of the occupied and unoccupied levels are at most of the order of

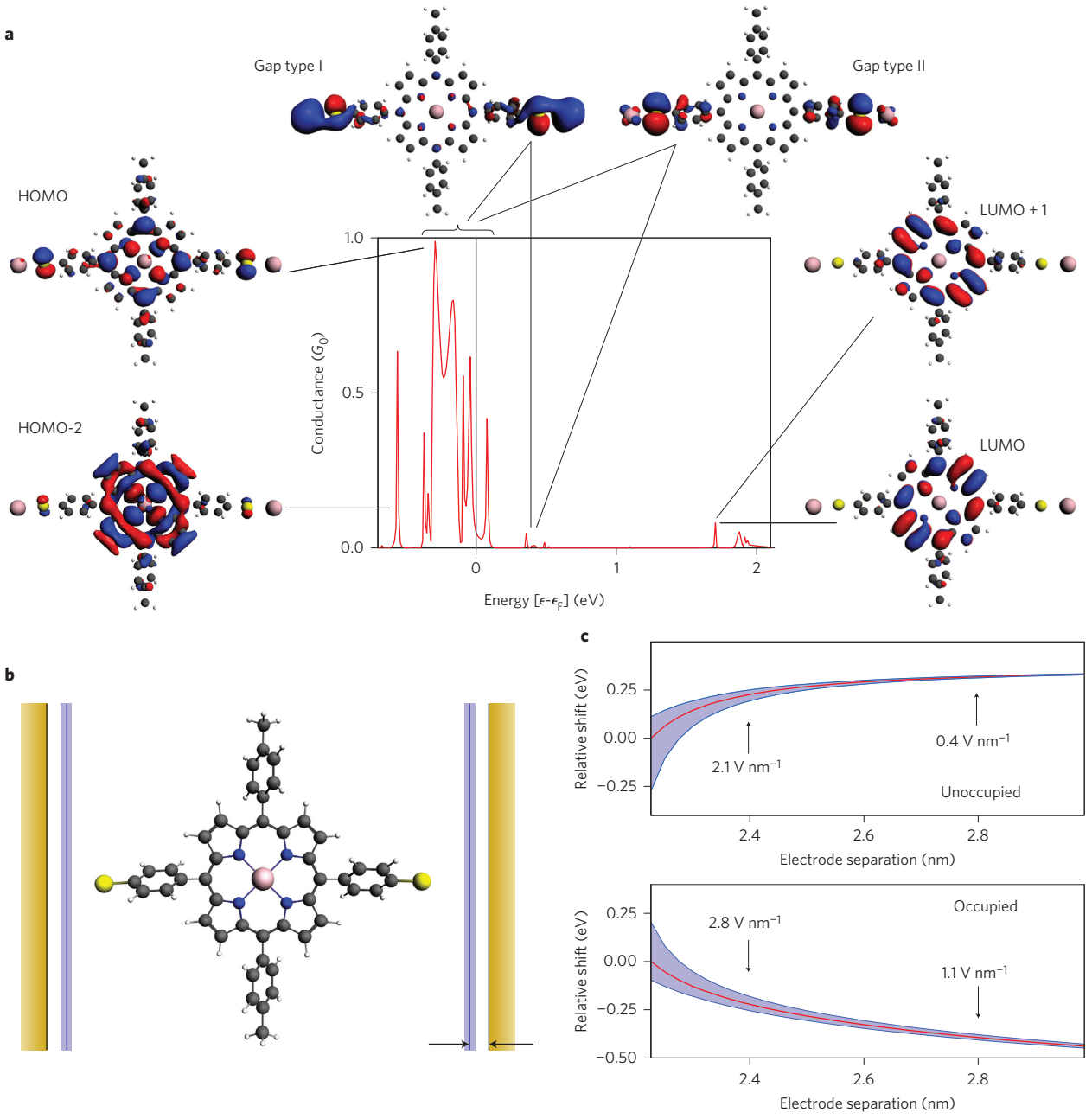

Figure 5 | Transport calculation and image-charge model. a, Zero-bias transmission and molecular orbital levels of ZnTPPdT coupled to gold, from DFT and DFT + NEGF calculations, respectively. The Fermi energies are reported with respect to the Fermi energy of the metal electrodes, which is marked by the vertical black line. ZnTPPdT is located 2.59 Å from each lead, with hollow-site binding. **b**, Image-charge model geometry, with the image plane located 1 Å outside the first atomic layer (uncertainty bands derived from a 0.25 Å deviation), as indicated by the two arrows. **c**, Level shifts (relative to the relaxed junction with an electrode separation of 2.23 nm) predicted by the image-charge model (with uncertainties) showing the occupied and unoccupied levels both shifting towards ϵ_F for increasing electrode separation. The values in the plot represent the expected resonance shift in the experiments, assuming a symmetrically applied bias, and yield mechanical gate couplings in the range 0.4–2.8 V nm^{-1}. These values may be significantly reduced for realistic electrode geometries.

50–60 meV and, more importantly, do not lead to transport-gap renormalization; instead, they cause a uniform, upward shift. In addition, the HOMO is predicted to move up for increasing electrode spacing, while the experiments show the opposite trend.

We conclude that image-charge effects can largely explain the experimentally observed distance dependence of the position of the molecular orbital levels with respect to the Fermi level of the contacts. Our calculations further reveal that the contributions to the image-charge effect of the charge distribution in the reference state impact substantially (roughly half that of gap renormalization) on the mechanical gate coupling of the molecular orbital levels.

The time needed for forming image charges is associated with the plasma frequency of the metallic contacts, corresponding to an energy of a few eV. This is short enough to be relevant, even in co-tunnelling processes. In recent years, several attempts have been made to capture the image charge-induced gap renormalization using either single point charges[43,45] or atomic charge distributions[15,44,46] based on DFT results for gas-phase molecules. In the present system, however, it seems that the states used for electron transport are defined by the presence of the contacts. Therefore, taking the atomic charge distributions for the different charge states inside the junctions is the appropriate starting point for calculating image-charge effects.

Conclusion

In summary, we have studied the influence of electrode separation on the molecular orbital levels in porphyrin single-molecule junctions using electrostatically gated MCBJ devices. Using this method we have demonstrated experimentally a combined effect of mechanical and electrostatic gating of the molecular levels. We find that both occupied and unoccupied levels move significantly towards the Fermi level upon reduction of the electrode spacing. We attribute this effect predominantly to gap renormalization as a result of electron interaction with image charges in the metal leads. Our findings are corroborated by DFT-based calculations. The experiments show surprisingly large level shifts, suggesting that image-charge effects may be responsible for the large spread in conductance values that is often observed in single-molecule junctions. These effects should therefore be considered in quantitative comparisons between computations and experiment in single-molecule junctions. At present, calculations for molecular devices result at best in the prediction of trends, or they shed light on the possible transport mechanisms. Improvements in geometric and electrostatic control may bring quantitative agreement closer between the two. We have demonstrated that capturing the image-charge effects is a crucial step in this development. From a different perspective, the observed effects may be exploited to mechanically gate single molecules and thereby tune the alignment of the orbital levels with respect to the Fermi level.

Received 6 July 2012; accepted 1 February 2013;
published online 17 March 2013

References

1. Ishii, H., Sugiyama, K., Ito, E. & Seki, K. Energy level alignment and interfacial electronic structures at organic/metal and organic/organic interfaces. *Adv. Mater.* **11,** 605–625 (1999).
2. Koch, N. Energy levels at interfaces between metals and conjugated organic molecules. *J. Phys. Condens. Matter* **20,** 184008 (2008).
3. Braun, S., Salaneck, W. R. & Fahlman, M. Energy-level alignment at organic/metal and organic/organic interfaces. *Adv. Mater.* **21,** 1450–1472 (2009).
4. Hwang, J., Wan, A. & Kahn, A. Energetics of metal–organic interfaces: new experiments and assessment of the field. *Mater. Sci. Eng. R* **64,** 1–31 (2009).
5. Lange, I. *et al.* Band bending in conjugated polymer layers. *Phys. Rev. Lett.* **106,** 216402 (2011).
6. Broker, B. *et al.* Density-dependent reorientation and rehybridization of chemisorbed conjugated molecules for controlling interface electronic structure. *Phys. Rev. Lett.* **104,** 246805 (2010).
7. Otsuki, J. STM studies on porphyrins. *Coord. Chem. Rev.* **254,** 2311–2341 (2010).
8. Ishii, H. *et al.* Energy level alignment and band bending at model interfaces of organic electroluminescent devices. *J. Lumin.* **61,** 87–89 (2000).
9. Heimel, G., Romaner, L., Zojer, E. & Bredas, J-L. The interface energetics of self-assembled monolayers on metals. *Acc. Chem. Res.* **41,** 721–729 (2008).
10. Bruot, C., Hihath, J. & Tao, N. Mechanically controlled molecular orbital alignment in single molecule junctions. *Nature Nanotech.* **7,** 35–40 (2012).
11. Romaner, L., Heimel, G., Gruber, M., Bredas, J-L. & Zojer, E. Stretching and breaking of a molecular junction. *Small* **2,** 1468–1475 (2006).
12. Amy, F., Chan, C. & Kahn, A. Polarization at the gold/pentacene interface. *Org. Electron.* **6,** 85–91 (2005).
13. Kubatkin, S. *et al.* Single-electron transistor of a single organic molecule with access to several redox states. *Nature* **425,** 698–701 (2003).
14. Osorio, E. *et al.* Addition energies and vibrational fine structure measured in electromigrated single-molecule junctions based on an oligophenylenevinylene derivative. *Adv. Mater.* **19,** 281–285 (2007).
15. Kaasbjerg, K. & Flensberg, K. Strong polarization-induced reduction of addition energies in single-molecule nanojunctions. *Nano Lett.* **8,** 3809–3814 (2008).
16. Thygesen, K. S. & Rubio, A. Renormalization of molecular quasiparticle levels at metal–molecule interfaces: trends across binding regimes. *Phys. Rev. Lett.* **102,** 046802 (2009).
17. Barr, J. D., Stafford, C. A. & Bergfield, J. P. Effective field theory of interacting π electrons. *Phys. Rev. B* **86,** 115403 (2012).
18. Champagne, A., Pasupathy, A. & Ralph, D. Mechanically adjustable and electrically gated single-molecule transistors. *Nano Lett.* **5,** 305–308 (2005).
19. Martin, C. A., van Ruitenbeek, J. M. & van der Zant, H. S. J. Sandwich-type gated mechanical break junctions. *Nanotechnology* **21,** 265201 (2010).
20. Parks, J. J. *et al.* Mechanical control of spin states in spin-1 molecules and the underscreened kondo effect. *Science* **328,** 1370–1373 (2010).
21. Meisner, J. S. *et al.* A single-molecule potentiometer. *Nano Lett.* **11,** 1575–1579 (2011).
22. Toher, C. *et al.* Electrical transport through a mechanically gated molecular wire. *Phys. Rev. B* **83,** 155402 (2011).
23. Kim, Y. *et al.* Conductance and vibrational states of single-molecule junctions controlled by mechanical stretching and material variation. *Phys. Rev. Lett.* **106,** 196804 (2011).
24. Van Ruitenbeek, J. M. *et al.* Adjustable nanofabricated atomic size contacts. *Rev. Sci. Instrum.* **67,** 108–111 (1996).
25. Kergueris, C. *et al.* Electron transport through a metal–molecule–metal junction. *Phys. Rev. B* **59,** 12505–12513 (1999).
26. Reichert, J., Ochs, R., Beckmann, D., Weber, H. B., Mayor, M. & von Lohneysen, H. Driving current through single organic molecules. *Phys. Rev. Lett.* **88,** 176804 (2002).
27. Dulić, D. *et al.* One-way optoelectronic switching of photochromic molecules on gold. *Phys. Rev. Lett.* **91,** 207402 (2003).
28. Martin, C. *et al.* Fullerene-based anchoring groups for molecular electronics. *J. Am. Chem. Soc.* **130,** 13198–13199 (2008).
29. Ruben, M. *et al.* Charge transport through a cardan-joint molecule. *Small* **4,** 2229–2235 (2008).
30. Wu, S. *et al.* Molecular junctions based on aromatic coupling. *Nature Nanotech.* **3,** 569–574 (2008).
31. Cuevas, J. C. & Scheer, E. *Molecular Electronics: An Introduction to Theory and Experiment* Ch. 13 (World Scientific, 2010).
32. Perrin, M. *et al.* Charge transport in a zinc-porphyrin single-molecule junction. *Beilstein J. Nanotechnol.* **2,** 714–719 (2011).
33. Dulić, D. *et al.* Controlled stability of molecular junctions. *Angew. Chem. Int. Ed.* **48,** 8273–8276 (2009).
34. Perrin, M. *et al.* Influence of the chemical structure on the stability and conductance of porphyrin single-molecule junctions. *Angew. Chem. Int. Ed.* **50,** 11223–11226 (2011).
35. Verzijl, C. J. O. & Thijssen, J. M. A DFT-based molecular transport implementation in ADF/band. *J. Phys. Chem. C* **116,** 24393–24412 (2012).
36. Xue, Y. & Ratner, M. Microscopic theory of single-electron tunneling through molecular-assembled metallic nanoparticles. *Phys. Rev. B* **68,** 115406 (2003).
37. Nara, J., Geng, W. T., Kino, H., Kobayashi, N. & Ohno, T. Theoretical investigation on electron transport through an organic molecule: effect of the contact structure. *J. Chem. Phys.* **121,** 6485–6492 (2004).
38. Pontes, R. B., Rocha, A. R., Sanvito, S., Fazzio, A. & da Silva, A. J. R. *Ab initio* calculations of structural evolution and conductance of benzene-1,4-dithiol on gold leads. *ACS Nano* **5,** 795–804 (2011).
39. Garcia-Lastra, J. M., Rostgaard, C., Rubio, A. & Thygesen, K. S. Polarization-induced renormalization of molecular levels at metallic and semiconducting surfaces. *Phys. Rev. B* **80,** 245427 (2009).
40. Myohanen, P., Tuovinen, R., Korhonen, T., Stefanucci, G. & van Leeuwen, R. Image charge dynamics in time-dependent quantum transport. *Phys. Rev. B* **85,** 075105 (2012).
41. Martin, R. M. *Electronic Structure: Basic Theory and Practical Methods* Ch. 10 (Cambridge Univ. Press, 2004).
42. Smith, N., Chen, C. & Weinert, M. Distance of the image plane from metal surfaces. *Phys. Rev. B* **40,** 7565–7573 (1989).
43. Quek, S. *et al.* Amine–gold linked single-molecule circuits: experiment and theory. *Nano Lett.* **11,** 3477–3482 (2007).
44. Kaasbjerg, K. & Flensberg, K. Image charge effects in single-molecule junctions: breaking of symmetries and negative-differential resistance in a benzene single-electron transistor. *Phys. Rev. B* **84,** 115457 (2011).
45. Neaton, J. B., Hybertsen, M. S. & Louie, S. G. Renormalization of molecular electronic levels at metal–molecule interfaces. *Phys. Rev. Lett.* **97,** 216405 (2006).
46. Mowbray, D. J., Jones, G. & Thygesen, K. S. Influence of functional groups on charge transport in molecular junctions. *J. Chem. Phys.* **128,** 111103 (2008).

Acknowledgements

This research was carried out with financial support from the Dutch Foundation for Fundamental Research on Matter (FOM) and the European Union Seventh Framework Programme (FP7/2007-2013, under grant agreement no 270369, 'ELFOS'). The authors would like to thank R. van Egmond for expert technical support and J. S. Seldenthuis for fruitful discussions.

Author contributions

D.D. and H.v.d.Z. designed the project. C.M., H.v.d.Z. and J.v.R. designed the set-up and the devices. M.P. and C.M. fabricated the devices. A.S., R.E. and J.v.E provided the molecules. M.P and D.D. performed the experiments. C.V., M.P. and J.T. performed the calculations. M.P., C.V., D.D., J.T. and H.v.d.Z. wrote the manuscript. All authors discussed the results and commented on the manuscript.

Additional information

Supplementary information is available in the online version of the paper. Reprints and permissions information is available online at www.nature.com/reprints. Correspondence and requests for materials should be addressed to H.v.d.Z.

Competing financial interests

The authors declare no competing financial interests.